

PROCEEDINGS OF SPIE

SPIDigitalLibrary.org/conference-proceedings-of-spie

Modelling reservoir turbidity from medium resolution Sentinel-2A/MSI and Landsat-8/OLI satellite imagery

Ouma, Yashon

Yashon O. Ouma, "Modelling reservoir turbidity from medium resolution Sentinel-2A/MSI and Landsat-8/OLI satellite imagery," Proc. SPIE 11528, Remote Sensing for Agriculture, Ecosystems, and Hydrology XXII, 115280J (20 September 2020); doi: 10.1117/12.2579319

SPIE.

Event: SPIE Remote Sensing, 2020, Online Only

Modelling Reservoir Turbidity from Medium Resolution Sentinel-2A/MSI and Landsat-8/OLI Satellite Imagery

Yashon O. Ouma^{*a}

^aDept. of Civil Engineering, University of Botswana, Private Bag 0061 UB, Gaborone, Botswana

ABSTRACT

This study investigates the use of Sentinel-2A (S2A) and Landsat-8 (L8) OLI for monitoring of turbidity in reservoir waters. Using observed *in situ* data from 18 sampling stations for Chebara Reservoir in Kenya, the study developed an empirical multivariate regression model for turbidity estimation from atmospherically corrected, band adjusted and spectral resolution standardized S2A and L8 bands. Best results for turbidity estimation were obtained from the regression of *in situ* data with B2 (blue) and B3 (green) bands as $[Rrs(B2/B3)^2 + Rrs((B2/B3))]$ for S2A and $[Rrs((B3/B2))]$ for L8. Both S2A and L8 retrieved turbidity with high and nearly equal accuracy of $R^2 > 0.75$ from the visible and NIR bands, with nearly similar RMSE of 0.5 NTU and NMAE% being higher for S2A by more than 30% as compared to L8's average NMAE% of 15%. The study shows that for both S2A and L8 sensors, and the proposed empirical regression algorithm suffices in the rapid and cost-effective quantification of turbidity inland reservoir waters. Using spatial interpolation for the visualization of the correlation between the predicted and observed turbidity, the L8 results were found to be more significant than the turbidity estimations using S2A bands.

Keywords: reservoir water quality; turbidity; Sentinel-2A/MSI; Landsat-8/OLI; Signal-to-Noise Ratio (SNR); Top of Atmosphere (TOA) reflectance; empirical multivariate regression modelling

1. INTRODUCTION

To monitor the water quality in reservoirs, the conventional water quality assessments through sampling and laboratory measurement is often employed. This conventional approach is however costly, prone to human and equipment errors, labor-intensive, time-consuming, and are not able to adequately assess the entire water body¹. To overcome the limitations in *in-situ* water quality monitoring methods, there is need for regular near-real-time, inexpensive, automated and non-invasive approaches, with adequate spatial-temporal coverages^{2,1}. Several studies have investigated the use of different satellite sensors for the assessment of water quality. Particularly the Landsat sensors have been widely used in the estimation of different water quality parameters (WQP)². For specific case studies and for the retrieval of water quality parameters (WQP), the previous studies have developed different correlational algorithms that are based on empirical models, semi-analytical models and matrix inversion models. Because of the drawbacks in semi-analytical and matrix inversion methods, empirical algorithms are often used for the retrieval and estimation water quality parameters^{3,2}.

In this study, the effectiveness of Sentinel-2A/MSI (S2A) and Landsat-8/OLI (L8) satellite sensors are demonstrated for the estimation of turbidity in a large reservoir (case-2 water body). Arguably, the medium-spatial resolutions satellite sensors, Landsat-8 OLI and Sentinel-2A MSI are capable of promoting more precise mapping of bio-optically active water quality parameters in recent times⁴. However, because of their differences in the spectral and spatial samplings, it is important to evaluate how well they are suited for the retrieval of water quality parameters. The current study has two objectives: (1) to identify the most suitable spectral bands (position and bandwidth) from the Sentinel-2A/MSI and Landsat-8/OLI sensors for accurate retrieval and estimations of turbidity, and (2) develop, test and validate empirical multivariate regression model algorithms for the estimation of the turbidity in case-2 waters.

2. DATA AND METHODS

2.1 Study area

The case study reservoir is the Chebara dam in Uasin Gishu County in Kenya and is located between longitudes 35° 29' 45.6"E and 35° 30' 7.2"E, and latitude of 0° 52' 55.2"S and 0° 53' 56.4"S. The dam was constructed in the 1990s to supply water to Eldoret Town situated 31 km away. The 2.1 km long dam has a capacity of 6.24 million cubic meters and is served by River Moiben and other small rivers and streams within the Chebara basin (Figure 1). Most of the rivers

Remote Sensing for Agriculture, Ecosystems, and Hydrology XXII, edited by Christopher M. U. Neale, Antonino Maltese, Proc. of SPIE Vol. 11528, 115280J · © 2020 SPIE
CCC code: 0277-786X/20/\$21 · doi: 10.1117/12.2579319

and streams flowing into the dam are permanent. Sparsely settled, agriculture is the main economic activity within the basin, with the rest of the land-cover being forest, grass and shrubs (Figure 1(a) and Figure 1(b)). The sampling stations were selected as shown in Figure 1, with the location and concentration of the sampling stations being based on the depth variations of the dam. 18 spatially distribute sampling stations were selected, 10 for the calibration of empirical regression algorithm, 5 for validation and 3 for off-season algorithm validation.

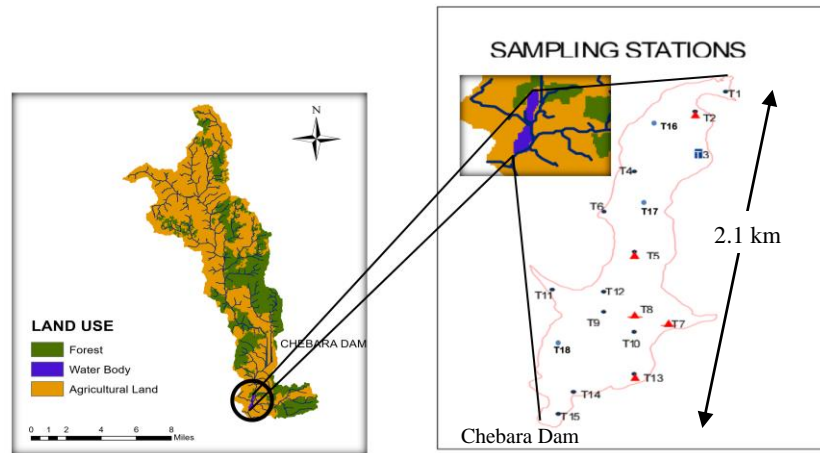


Figure 1. Chebara Basin, land-use and land-cover and the sampling points.

Table 1. Spectral and spatial samplings of the visible, NIR and SWIR bands in Landsat-8 OLI and Sentinel-2A MSI.

Landsat-8 OLI				Sentinel-2A MSI			
Band # and Spectral Range	Spectral Resolution (nm)	Band width (nm)	Spatial Resolution (m)	Band # and Spectral Range	Spectral Resolution (nm)	Band width (nm)	Spatial Resolution (m)
B1-Coastal aerosol	435–451	16	30	B1-Coastal aerosol	433–453	21	60
B2-Blue	452–512	60	30	B2-Blue	458–523	66	10
B3-Green	533–590	57	30	B3-Green	543–578	36	10
B4-Red	636–673	37	30	B4-Red	650–680	31	10
B5-NIR	851–879	28	30	B8-NIR	785–900	106	10
				B9-NIR Narrow	855–875	21	20
B6-SWIR1	1566–1651	85	30	B11-SWIR 1	1566–1655	91	20
B7-SWIR2	2107–2294	187	30	B12-SWIR 2	2100–2280	175	20

2.2 Sentinel-2A MSI sensor

The Sentinel-2 mission comprises of twin polar-orbiting satellites, Sentinel-2A and Sentinel-2B, which were respectively launched on 23 June, 2015 and 7 March, 2017. Each Sentinel-2 satellite carries a multispectral instrument (MSI), with swath width of approximately 290 km, spatial high resolutions in 10 m, 20 m and 60 m, with a revisit time of 10-days with one satellite and 5-days with two satellites at the equator. The Sentinel-MSI has 13 spectral bands (430 nm to 2320 nm) in the visible, red-edge, near-infrared, and shortwave infrared regions of the spectrum (Table 1). With high-temporal resolution and 12-bit radiometric resolution, like the Landsat-8 sensor, the MSI sensor provides high radiometric dynamics for the observed areas of both the very dark e.g. water surfaces and the very bright areas e.g., ice and snow. For comparison with the Sentinel-2A MSI, only the similar spectral bands in Landsat-OLI are analyzed as presented in Table 1. For the Sentinel-2A, the level 1C is corrected for atmospheric errors using the Sentinel’s SNAP algorithm, resulting in the level 2A product of Sentinel-2 from the Sen2Cor processor, which includes scene classification and atmospheric correction.

2.3 Landsat-8 OLI sensor

The Landsat-8 mission carries the Operational Land Imager (OLI) and the Thermal InfraRed Sensor (TIRS). OLI collects image data for nine shortwave bands with spatial sampling or resolution of 30-meters (bands 1-7) and the panchromatic band with pixel size of 15 meters (band 8) (Table 1). TIRS collects data for two long-wave thermal bands at 100 meters (band 9) every 16 days which are resampled to 30 meters to match OLI multispectral bands. The OLI sensor is compatible with the earlier Landsat sensors, and presents improved measurement capabilities. Compared to the Landsat-7/ETM+, the Landsat-8/OLI (Table 1) has improved radiometric resolution with reduced image noise and spectral heterogeneity. This is observed to be particularly significant in precise water surface extraction and water quality retrievals. This study utilized Landsat-OLI data acquired on the 22nd January 2019 and the Sentinel-2A satellite image acquired on 25th January 2019. The fieldwork was carried out during the dry season and coincided with the sensors acquisitions from 23th to 24th January 2019.

2.4 TOA reflectance derivation and Signal-to-Noise Ratio analysis

To derive and compare the top of atmosphere (TOA) reflectance from the optical sensors, for Landsat-8 level-1 the digital numbers from each band (B_{L8}) are converted to TOA reflectance using the Landsat-8 metadata scaling factors, and dividing by the cosine of the solar zenith angle. In addition, Landsat per-pixel solar and viewing angles were calculated using the Landsat 8 Angles Creation Tool provided by USGS (<https://landsat.usgs.gov/solar-illumination-and-sensor-viewing-anglecoefficient-file>), and the angle coefficient file available with each Collection 1 L1TP file. For the Sentinel-2 MSI, the TOA reflectance and solar view geometry are stored in the metadata for every 5 km. Further, to understand the impact of noise in turbidity estimations, the sensor bands were compared in terms of the signal-to-noise ratios SNR spectral bandwidths using the area mean to standard deviation ($SNR = \mu / \sigma$) ratio.

2.5 Empirical regression modelling for retrieval of water quality parameters

Using empirical regression modelling, simulations are carried out to establish the multivariate correlations between the sensors bands reflectances and the measured *in-situ* water quality variables. The multivariate regression model for estimating the water quality parameters in the reservoir is developed by determining the quantitative relationships between the measured *in situ* water quality parameter and the and remote sensing reflectance from the satellite spectral data. The empirical models used comprised of the following model equations, linear: $a * R_{rs}(\lambda) + b$; polynomial: $a * R_{rs}(\lambda)^2 + b * R_{rs}(\lambda) + c$; logarithmic: $a * \log_{10} R_{rs}(\lambda) + b$; power: $a * R_{rs}^b(\lambda)$ and exponential: $a * e^{b * R_{rs}(\lambda)}$, where $R_{rs}(\lambda)$ is the corresponding remote sensing reflectance for L8 (B_{L8}) and S2A (B_{S2A}) bands and a , b and c are the regression model constants. The models were evaluated using the following performance metrics:

$$R = \frac{\sum_{i=1}^n (y_i - \bar{y}) \cdot (x_i - \bar{x})}{\sqrt{\sum_{i=1}^n (y_i - \bar{y})^2 \cdot \sum_{i=1}^n (x_i - \bar{x})^2}} \quad (1)$$

$$RMSE = \sqrt{\frac{1}{n} \sum_{i=1}^n (x_i - y_i)^2} \quad (3)$$

$$MAE = \frac{1}{n} \sum_{i=1}^n |x_i - y_i| \quad (2)$$

$$NMAE\% = \left[\frac{1}{n} \sum_{i=1}^n \frac{|x_i - y_i|}{x_i} \right] * 100 \quad (4)$$

3. RESULTS AND DISCUSSIONS

3.1 Sentinel-2 MSI and Landsat-8 OLI TOA reflectance comparison

In comparing the TOA and surface reflectance from the two sensors, the spatial subsets (A and B) for the selected water bodies are shown in Figure 2(a). In terms of the inter-band spectral responses for the selected water body areas, the scatterplots between the Landsat-OLI and Sentinel-2A spectral bands showed a high correlation of $R^2 > 0.876$, for all the

seven homologue bands in Table 1. The regression plots in Figure 2(a) presents sample results from the correlations between the red and NIR bands from the spatial subset of the two water body scenes A and B. The red and NIR bands represent the reflectance in the visible and NIR, which are commonly used in water quality modelling^{2,6,7,8}. The regression results indicate that the two sensors contain nearly similar spectral radiance information, despite the marginal difference in the SNR. Figure 2(a) shows that for the same scene water body, the sensors have a close cross-correlation in the red and NIR bands, which is also observed in the TOA reflectance plot in Figure 2(b) with the TOA from Landsat-OLI wavelengths being slightly higher than from Sentinel-2A bands. The moderately higher TOA reflectance in Landsat-OLI confirms the higher SNR. The results in Figure 4 show that the Landsat-OLI bands present a slightly higher TOA reflectance than the Sentinel-2A bands.

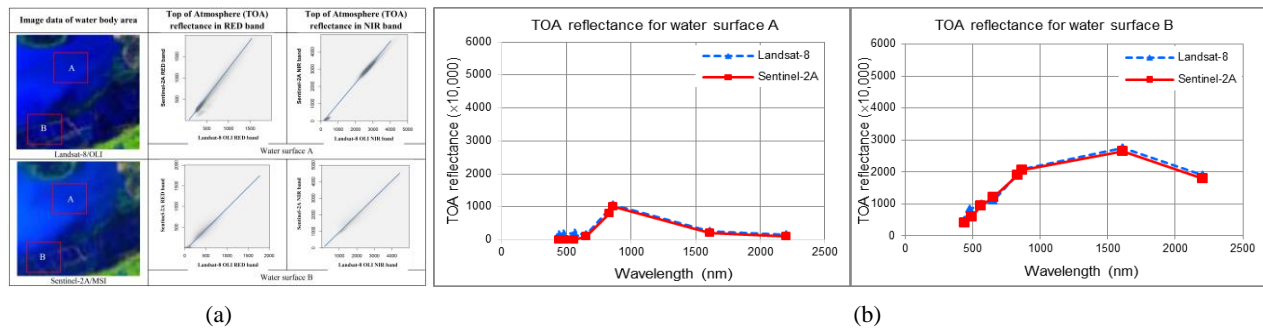


Figure 2. (a) SNR on clear water bodies in the visible and NIR bands from Sentinel-2A MSI and Landsat-8 OLI. (b) Comparison between TOA reflectance from Landsat-8 OLI and Sentinel-2A MSI for clear water surfaces.

3.2 Signal-to-Noise Ratio (SNR) on clear water bodies

From the spatially uniform and clear water bodies, the Sentinel-2A and Landsat-OLI SNR radiometric performance were determined for the visible and NIR bands⁵. Figure 3 shows the SNR computed from the average of local window area from the ratio of the area mean to standard deviation ($SNR = \mu / \sigma$). The SNR is determined using a 3x3 pixel-kernel on the mean TOA. The selected water body areas are outlined in Figure 2(a) corresponding to spatial areas A and B.

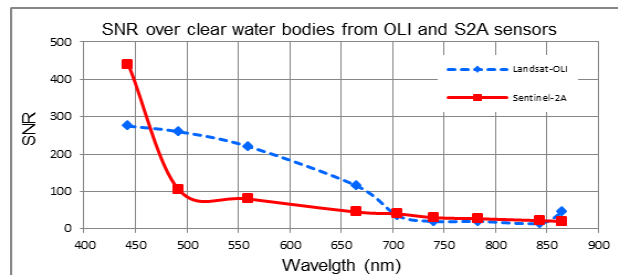


Figure 3. The TOA reflectance correlation scatterplots from Landsat-OLI and Sentinel-2A reflectance in red and near-infrared for clear water surfaces (A and B).

In the three visible bands blue (490 nm), green (560 nm) and red (665 nm), the Landsat-OLI bands exhibit SNR values of 2–3 times higher than the corresponding MSI bands. In the coastal aerosol bands (443 nm), MSI is at approximately 30% higher than OLI in SNR. Theoretically therefore, it can be inferred that since SNR is proportional to the square root of the area of a pixel, then the aggregated 20 m – 30 m spatial resolution of the MSI bands should be able offer similar or better radiometric quality in the visible bands as compared to the OLI bands for the clear water areas.

3.3 Estimation of turbidity concentration in reservoir waters

From the empirical multivariate regression modelling comparing the satellite reflectance data and the laboratory measured water quality factor, the study results show that the turbidity was estimated from the two sensors with the same accuracy of $R^2 > 0.75$ (Figure 4). For both the sensors, the visible bands (blue, green and red) are observed to be predominant in the retrieval of turbidity within the reservoir. In Figure 4, the best estimate of turbidity using Sentinel-2A is at $R^2 = 0.8004$, which is comparable to turbidity estimates using Landsat-OLI with $R^2 = 0.8134$. The models accurately predicted the concentrations of turbidity from both sensors as the RMSE and bias error measures were less than the minimum and average *in situ* turbidity. The turbidity estimation results are particularly important since turbidity is considered as one of the most significant water quality parameters⁹. For the assessment of the extraction of turbidity as the significant water quality parameter that relates directly to the underwater light penetration that affects productivity,⁹ showed from several band combinations that Landsat-OLI band 4 (red) has the best correlation with the *in-situ* measured turbidity with a coefficient of determination R^2 of 0.84, and scatter index of 0.22 and RMSE of 0.28 NTU.¹⁰ also recently demonstrated using multivariate regression model and gene-expression programming (GEP) that reservoir turbidity could be extracted with R^2 of greater than 90%, using the combination of visible and NIR bands. While high accuracy has been observed in turbidity estimation, in all the studies, atmospheric correction was found to be a factor in the accuracy of the WQP modelling³.

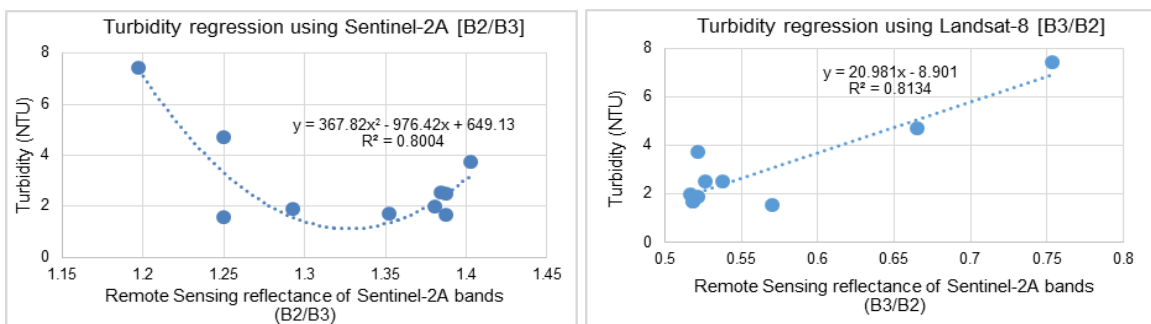


Figure 4. Left: Laboratory measured Turbidity and Sentinel-2A band reflectance: RMSE = 0.3272NTU, MAE (Bias) = 0.0691NTU and MAPE = 10.71%. Right: Landsat band reflectance and *in-situ* Turbidity measurements. RMSE = 0.4024NTU, MAE (Bias) = 0.1475NTU and MAPE = 14.72 %.

From the laboratory measurements, the turbidity the turbidity is observed to vary from 1.36 NTU to 7.42 NTU and averaging at 2.83 NTU, implying the reservoir is characterized by low turbid waters. The low turbidities could be attributed to low flows into the reservoir, especially during the dry period when the water samples were collected. With minimum inflow of sediment laden rainwater discharge and the slow velocities of the river water, the concentrations of sediments that would cause reservoir turbidity was low. Further, at a maximum depth of approximately 150 m, the reservoir depth enables the settlement of sediments at the bottom of the reservoir with minimal potential of re-suspension by water currents and waves. The higher degree of settling of sediments therefore leads to low turbidity in the reservoir.

The validation of the developed regression models was carried out using the five (5) sampling stations (T2, T5, T7, T8, T13) in Figure 1. The validation results are presented in Table 2, including the statistics from the stations which were used in the model calibration. From the SD, CV and SE metrics, Landsat-OLI tended to underestimate the turbidity, while Sentinel-2A based models tended to overestimate the same WQP, thus predicting the parameters with a higher coefficient of variation.

Table 2. Descriptive statistics of the laboratory measured and predicted water quality parameters. (SD = standard deviation; CV= coefficient of variation and SE = standard error).

Water quality parameter and estimation and data source	Sample (n)	Min	Max	Median	Average	SD	CV (%)	SE	
Turbidity (NTU)	<i>In situ</i> WQP measurements	15	1.36	7.42	1.97	2.83	1.69	59.64	0.42
	Landsat-8 OLI	15	1.94	6.92	2.05	2.88	1.46	50.77	0.38
	Sentinel-2A MSI	15	1.23	26.25	2.48	4.99	6.51	130.52	1.68

To understand the distribution of turbidity within the reservoir, Figure 5 presents the spatial interpolation results using ordinary Kriging. It is observed that the spatial deviations of the Sentinel-2A estimates indicated overestimated turbidity

concentration, while Landsat-OLI estimations are closely correlated in spatial location and areal distribution with the laboratory measured turbidity. Notably, though the statistical analysis shows that both sensors detected the turbidity with accuracy of more than 75%. This implies for such estimations, the visualization of the distribution of the predicted phenomenon is significant in addition to the statistical measures of accuracy.

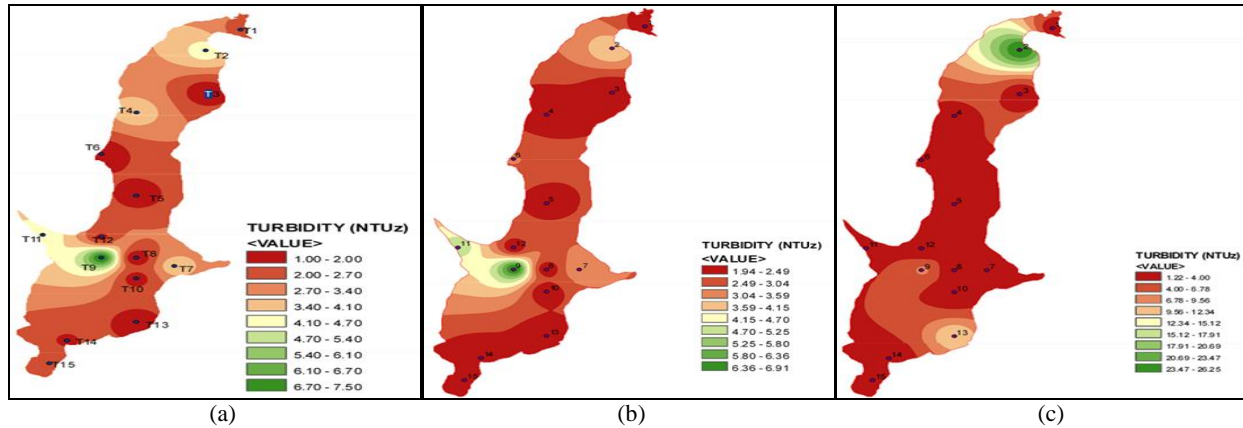


Figure 5. Spatial distribution of turbidity concentration from (a) *in-situ* sampling and laboratory measurements, and from the model predictions using (b) Landsat-8 OLI and (c) Sentinel-2A MSI for Chebara dam.

4. CONCLUSIONS

This study compared Landsat-8 OLI and Sentinel-2A MSI satellite sensors for the estimation of turbidity in an inland water reservoir. For clear water surfaces, Landsat-8 exhibited higher signal-to-noise ratio (SNR) in the visible bands, and a marginally higher water surface reflectance in the visible and NIR bands as compared to the corresponding Sentinel-2A bands. Using the visible and NIR bands with the empirical multivariate regression model, the presence of turbidity was retrieved from Sentinel-2A and turbidity with nearly equal accuracy of more than 75% as measured with R^2 . The statistical analysis results demonstrates the potentials of using both sensors in reservoir water turbidity retrieval, however the study recommends that further visualization analysis should be carried out to ascertain the actual spatial distribution of the predicted water quality parameter in comparison with the laboratory measurements.

REFERENCES

- [1] Ouma, Y. O., Okuku, C. O., Njau, E.N., "Use of Artificial Neural Networks and Multiple Linear Regression Model for the Prediction of Dissolved Oxygen in Rivers: Case Study of Hydrographic Basin of River Nyando, Kenya," *Complexity*, 2020, Article ID9570789, 23pages (2020).
- [2] Ouma, Y. O., Waga, J., Okech, M., Lavisa, O., Mbuthia, D., "Estimation of reservoir bio-optical water quality parameters using Smartphone Sensor Apps and Landsat ETM," *Journal of Sensors*, 2018, Article ID 3490757, 32 pages (2018).
- [3] Toming, K., Kutser, T., Laas, A., Sepp, M., Paavel, B., Noges, T., "First Experiences in Mapping Lake Water Quality Parameters with Sentinel-2 MSI Imagery," *Remote Sensing*, 8(8), 640 (2016).
- [4] Tyler, A. N., Hunter, P. D., Spyrakos, E., Groom, S., Constantinescu, A. M., Kitchen, J., "Developments in Earth observation for the assessment and monitoring of in-land, transitional, coastal and shelf-seawaters," *Science of the Total Environment*, 572, 1307–1321 (2016).
- [5] Drusch, M., Del Bello, U., Carlier, S., Colin, O., Fernandez, V., Gascon, F., Hoersch, B., Isola, C., Laberinti, P., Martimort, P., "Sentinel-2: ESA's optical high-resolution mission for GMES operational services," *Remote Sensing of Environment*, 120, 25–36 (2012).
- [6] Yepez, S. et al., "Retrieval of Suspended Sediment Concentrations using Landsat 8 OLI Satellite Images in The Orinoc River. (Venezuela)," *Comptes Rendus Geoscience*, 350(1-2), 20-30 (2018).

- [7] Mushtaq, F., Lala, M. G., “Remote estimation of water quality parameters of Himalayan Lake (Kashmir) using Landsat 8 OLI Imagery,” *Geocarto International*, 32(3), 274-285 (2016).
- [8] M. Banansea, M. Ledesma, C. Rodriguez, and L. Pinotti, “Using New Remote Sensing Satellites for Assessing Water Quality in a Reservoir,” *Hydrological Sciences Journal*, 64(1), 34–44 (2017).
- [9] Quang, N. H., Sasaki, J., Higa, H., Huan, N. H., “Spatiotemporal Variation of Turbidity based on Landsat 8 OLI in Cam Ranh Bay and Thuy Trieu Lagoon, Vietnam,” *Water*, 9(8), 570 (2017).
- [10] Liu, L-W., Wang, Y-M., “Modelling Reservoir Turbidity Using Landsat 8 Satellite Imagery by Gene Expression Programming,” *Water*, 11(1479), 2019.